ACS OMEGA

Open Access

http://pubs.acs.org/journal/acsodf

Article

Highly Porous 3D Ni-MOFs as an Efficient and Enzyme-Mimic Electrochemical Sensing Platform for Glucose in Real Samples of Sweat and Saliva in Biomedical Applications

Rajaji Pavadai, Mani Arivazhagan, Jaroon Jakmunee, Nethaji Pavadai, Revathi Palanisamy, Ganesha Honnu, Sutasinee Kityakarn, Jeerawan Khumphon, Chaisak Issro, Dusadee Khamboonrueang, and Sirikanjana Thongmee*

Cite This: *ACS Omega* 2025, 10, 1610−1623

Read Online

ACCESS | Metrics & More | Article Recommendations | Supporting Information

ABSTRACT: Nickel-based metal−organic frameworks, denoted as three-dimensional nickel trimesic acid frameworks (3D Ni-TMAF), are gaining significant attention for their application in nonenzymatic glucose sensing due to their unique properties. Ni-MOFs possess a high surface area, tunable pore structures, and excellent electrochemical activity, which makes them ideal for facilitating electron transfer and enhancing the catalytic oxidation of glucose. This research describes a new electrochemical enzyme-mimic glucose biosensor in biological solutions that utilizes 3D nanospheres Ni-TMAF created layer-by-layer on a highly porous nickel substrate. The Ni-TMAF based on the nonenzymatic electrochemical glucose oxidation represent the promising approach, leveraging the unique properties of Ni-TMAF to provide efficient, stable, and potentially more cost-effective alternatives to traditional enzyme-mimic sensors. The MOF is synthesized from trimesic acid (TMA) and nickel nitrate hexahydrate through a solvothermal reaction process. The resulting Ni-TMAF utilizes the three-dimensional nanospheres of crystalline porous structure with a large surface area and numerous active sites for catalytic reaction toward glucose. Ni-TMAF are indeed known for their excellent electrocatalytic activity, particularly in the context of glucose oxidation under alkaline conditions. The nickel centers in the Ni-TMAF facilitate efficient electron transfer and redox reactions, leading to the high sensitivity of 203.89 μA μM^{-1} cm^{-2} and lower LOD of 0.33 μM and fast response time of <3 s in glucose sensors. Their stability, cost-effectiveness, and high performance make 3D Ni-TMAF a promising material for nonenzymatic electrochemical glucose sensors.

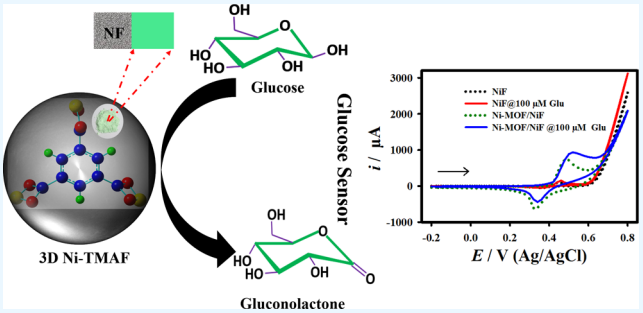

1. INTRODUCTION

Glucose is a fundamental organic molecule that serves as the primary energy source for cellular metabolism in humans.[1] Glucose plays a crucial role in both medical diagnostics and the food industry, driving significant interest in its rapid and accurate analysis. In medical diagnostics, precise glucose monitoring is essential for managing diabetes, where maintaining blood sugar levels within a target range is critical for preventing complications.[2,3] Maintaining the glucose concentration within the normal range is crucial for metabolic health. The normal blood glucose levels for healthy individuals typically range between 3.9 and 6.1 mM (70−110 mg/dl).[4] Rapid glucose analysis allows for real-time decision-making, improving patient outcomes and enabling better disease management. In the food industry, glucose levels can influence product quality and safety, making its accurate measurement important for manufacturing processes, product development, and ensuring compliance with nutritional labeling regulations.[5,6] The growing demand for quick and reliable glucose detection has spurred advancements in sensor technologies, particularly nonenzymatic electrochemical sensors, which offer high sensitivity, selectivity, and rapid response times. These innovations are pivotal in enhancing the efficiency and effectiveness of glucose monitoring across various applications.

Diabetes is an increasingly widespread worldwide public disease caused by high blood glucose concentrations. Neural impairment, kidney failure, and neurological and cardiovascular disorders are examples of related problems.[7,8] Blood glucose tests that are regulated and conducted regularly can help prevent these issues. Electrochemical research has gained popularity in comparison to conductometry, colorimetry, and

Received: October 17, 2024
Revised: December 5, 2024
Accepted: December 6, 2024
Published: December 27, 2024

fluorescence spectroscopy due to its simple fabrication process and equipment downsizing.[9,10] A current or voltage output can quantitatively describe the degree of electrooxidation of glucose. Enzymatic electrochemical glucose sensors are available on the market to detect glucose levels.[11] Still, their prohibitive price and lack of stability limit their widespread adoption, allowing for the invention of nonenzymatic glucose sensors.[12,13]

Electroanalytical approaches offer significant advantages over other analytical methods when it comes to glucose detection and quantification. In comparison to optical or chromatographic methods, electroanalytical methods can detect glucose without the need for elaborate sample preparation or expensive reagents.[14,15] For instance, nonenzymatic glucose sensors, using materials like bimetal oxide, MoS_2, MXene-embedded porous carbon materials and metal−organic frameworks (MOFs), exhibit exceptional sensitivity and selectivity while maintaining the advantages of simplicity and affordability.[16−19] In summary, electrochemical approaches combine speed, simplicity, and cost-effectiveness, making them highly appealing for glucose detection, especially in point-of-care testing and continuous monitoring. These platforms have become essential in diagnostics, particularly in point-of-care and continuous monitoring scenarios.

Glucose electrooxidation is highly dependent on the electrode materials, according to the literature. Prior research has demonstrated the high efficiency of anode catalysts for glucose electrooxidation made of platinum, gold, palladium, and alloys of Pt, Pd, Au, and Ag.[20−22] Nevertheless, these materials are still very expensive and particularly vulnerable to the synergistic effect. Furthermore, non-noble catalysts for the glucose oxidation reaction (GOR), including cobalt, copper, iron, and nickel, have been explored as electrocatalytic elements. Regarding non-noble catalysts, nickel and nickel-based nanocomposites demonstrate good electrocatalytic performance in alkaline media because of their affordability, outstanding activity, and ability to promote electron transfer processes at lower overpotentials.[23−25] Furthermore, according to previously reported studies, nickel complexes exhibited exceptional catalytic abilities in the oxidation of alcohols in alkaline solutions and the production of NiOOH species. Therefore, high-efficiency porous coordination network (PCN)-based electrocatalysts are urgently required for glucose electrooxidation. In recent years, coordination polymers (CPs) and their special subgroups of metal−organic frameworks (MOFs) are considered a new category of electrocatalysts due to their incredible thermal and chemical durability, significant surface area, remarkable porosity, and three-dimensional structures.[26−29] Three-dimensional (3D) MOFs have a highly porous structure with an exceptionally high surface area and excellent intrinsic properties of chemical and thermal stability and facilitate efficient mass transport of ions and molecules, reducing diffusion limitations, which provides more active sites for electrochemical reactions. MOFs can be customized by altering their metal nodes and organic linkers to create hybrid structures that enhance conductivity, stability, and electrochemical performance, further allowing for selective binding or recognition of specific analytes. The presence of metal ions and surface functional groups in CPs and MOFs generates active sites and enhanced catalytic performance.[30,31] Although CPs/MOFs have accomplished great progress, their application in glucose monitoring has been limited by the low conductivity of the mixture of organic−inorganic polymers. For instance, they have been accepted for their catalytic activity in glucose electrochemical detection.[32−34]

With this strategy, the inherent advantages of MOFs for nonenzymatic sensor applications are to be leveraged while overcoming conductivity issues. These research efforts represent a significant advancement in the construction of MOF-incorporated glucose sensing systems.[35] In this article, we report a simple and inexpensive way to create coordination network nanospheres of Ni(II)-trimesic acid on an extremely porous Ni surface. The hybrid framework achieved an approximate 82% increase in anodic current densities against NiF, which consists of Ni(II) nodes bonded with a trimesic acid linker and exhibits strong electrocatalytic activity for glucose oxidation. In addition, the glucose can get robust oxidation with a slight shift in positive potential with good linear oxidation as well as wider concentration ranges from 100−2500 μM glucose. The resulting Ni-TMAF has abundant catalytically active sites. Moreover, the improved electrical and ionic conductivity of the Ni-TMAF-based electrodes and the uniform distribution of the Ni nanoparticles promote catalytic performance. The catalyst has high sensitivity and a wider linear detection range. Furthermore, we successfully used the Ni-TMAF nanosphere-modified NF electrodes to determine the broad potential for use as an actual glucose sensor. The Ni-TMAF nanosphere-modified NF electrodes have a strong potential for practical glucose sensing applications due to their broad linear detection range and high sensitivity.

2. EXPERIMENTAL SECTION

2.1. Chemicals. Nickel(II) nitrate hexahydrate ($Ni(NO_3)_2{\cdot}6H_2O$), poly(vinylidene fluoride) (PVDF), and trimesic acid (TMA) ($C_6H_3(CO_2H)_3$) were collected from Kemaus Chemicals. Solvents like C_2H_5OH and *N*,*N*-dimethylformamide (DMF) were collected from Sigma-Aldrich. Potassium hydroxide (KOH) was collected from Vijaya Scientific. A Millipore Milli-Q system was used to purify deionized water and was then utilized for all of the tests in this overall research. Nickel foam was collected from Thermo Fisher Scientific. Each chemical was analytical grade and was used with no further purification.

2.2. Synthesis of 3D Ni-TMAF. The 3D Ni-TMAF nanospheres were synthesized by the solvothermal technique (Scheme 1), as described in the literature.[36] First, 60 mL of DMF, 15 mL of deionized water, and 5 mL of absolute ethanol were poured into a 200 mL beaker and stirred for 5 min at 300 rpm. Next, an equal molar ratio (25 mmol) of $Ni(NO_3)_2{\cdot}6H_2O$ and TMA was added into the above solution and treated

Scheme 1. Schematic Diagram for the Synthesis of 3D Ni-TMAF

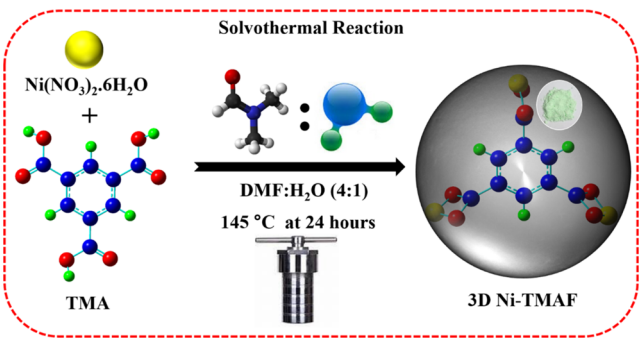

https://doi.org/10.1021/acsomega.4c09437
ACS Omega 2025, 10, 1610−1623

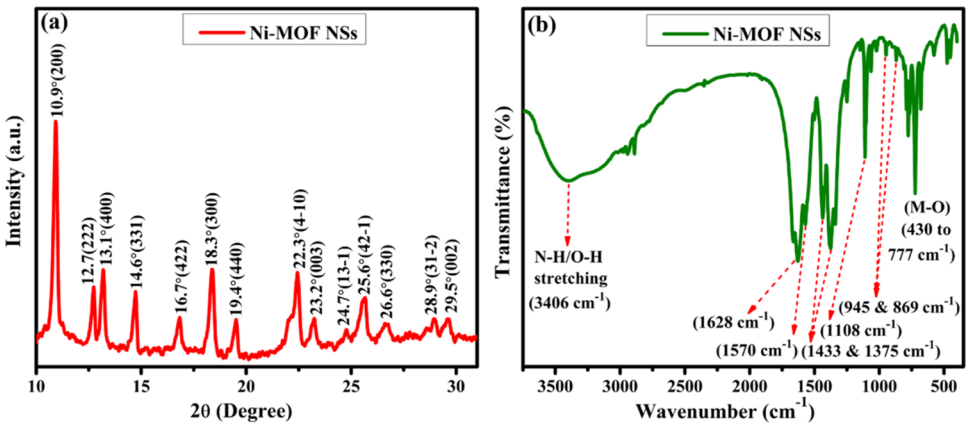

Figure 1. XRD (a) and FT-IR (b) spectra for 3D Ni-TMAF.

with sonication for 5 min. The resulting visible solution was transferred in a 100 mL Teflon-lined stainless steel autoclave and heated at 145 °C for 20 h. The precipitate was filtered after being cooled to ambient temperature. Further, the samples were continuously cleaned by DMF and dried for 12 h at 90 °C. Finally, 600 mg of light-green color 3D Ni-TMAF precipitate was collected.

2.3. Instrumentation Techniques. The crystalline behavior of 3D Ni-TMAF was investigated using an X-ray diffractometer (XRD, D8-Advanced Bruker) with Cu Kα radiation (λ = 1.5418 Å) in the theta range from 10 to 90°. The chemical bonds of 3D Ni-TMAF were examined through Fourier transform infrared spectroscopy (FT-IR, TENSOR 27 Bruker) at 4000−400 cm^{-1}. The morphology of the as-prepared material was obtained from field-emission scanning electron microscopy (FESEM, Hitachi SU8030-FESEM, Japan, functioned at 10−15 kV) and transmission electron microscopy (TEM, JEOL2100 Plus, Japan, functioned at 200 kV). X-ray photoelectron spectroscopy (Physical Electronics: PerkinElmer Phi 1600 ESCA) with a magnesium radiation basis was utilized to determine the chemical state of the 3D Ni-TMAF surface. The Raman spectra of 3D Ni-TMAF were obtained through a Raman spectrometer (LabRAM HR Evolution, Horiba). The thermogravimetric analysis instrument (PerkinElmer, Diamond) was used for evaluating the thermal properties of the 3D Ni-TMAF at a heating rate of 2 °C per minute. The Brunauer−Emmett−Teller technique (BET) was employed to measure the specific surface area and pore volume of the prepared material. All electroanalytical measurements were carried out using an Electrochemical EmStat4S/LR electrochemical interface workstation at a temperature of 26 ± 3 °C. The experiments employed a three-electrode system: the Ni-TMAF/NF served as the working electrode, a platinum (Pt) wire served as an auxiliary electrode, and an Ag/AgCl (3.0 M KCl) served as the reference electrode.

2.4. Electrode Preparation. The electrocatalytic effect of the synthesized material was investigated through a three-electrode system. The three-electrode system contained a working electrode, a reference electrode (Ag/AgCl), and a counter electrode (platinum wire). Ni foam was treated with 1 M HCl and then washed with distilled water, sonicated with ethanol for 15 min, and dried in an oven for 6 h. After that, the synthesized material was placed on a Ni foam substrate. The electrochemical reaction was investigated by combining active materials (80%), carbon black (10%), and PVDF (10%) as the binder material. After homogeneous mixing in NMP, the slurry was applied over nickel foam (0.2 × 0.2 mm^2). It was allowed to air out in an oven at 60 °C overnight. The dried foam's mass was measured and recorded for glucose sensor applications. The mass loading of the catalyst was found to be 1.8 mg/mm^2.

2.5. Real Sample Preparation. The collection of human sweat and saliva samples from a volunteer and their immediate refrigeration was essential to maintaining sample quality and ensuring the sensor's performance could be tested under realistic conditions. The sensor's potential for detection of glucose and noninvasive health monitoring is demonstrated by the encouraging findings of these tests, especially when it comes to monitoring the glucose levels in common, easily accessible fluids like sweat and saliva. This platform may be modified to track additional biomarkers in saliva and sweat, increasing its applicability in personalized medicine and health diagnostics. Centrifuging sweat and saliva samples is an essential step in preparing them for accurate electrochemical analysis, particularly for detecting glucose. After filtering, the supernatant was diluted approximately ten times with 1.0 M KOH. Without any additional pretreatment, the resultant solution was moved into the electrochemical cell for actual sample analysis. After being further diluted to produce 5.0, 10.0, and 20.0 μM glucose, a stock solution of glucose (1.0 mM) was kept refrigerated. The glucose concentrations in sweat and saliva samples were detected using the standard addition method (SAM), which ranged from 5.0 to 20.0 μM. The recovery test for the identification and quantification of glucose in human sweat and saliva samples was carried out using the chronoamperometric technique, which involved the addition of a specific glucose concentration in the real sample analysis.

3. RESULTS AND DISCUSSION

3.1. Materials Characterization. As-synthesized 3D Ni-TMAF were studied by using XRD, FT-IR, SEM, FE-TEM, EDAX, XPS, and BET analysis. In the XRD pattern (Figure 1a), the well-defined sharp peak of synthesized material indicates the crystalline nature. Typical diffraction peaks of 3D Ni-TMAF were obtained at 10.92° (200), 12.7° (222), 13.1° (400), 14.6° (331), 16.7° (422), 18.3° (300), 19.4° (440), 22.3° (4−10), 23.2° (003), 25.6° (42−1), 26.6° (330), 28.9° (31−2), and 29.5° (002) with the average crystalline size of 29.3 nm.[37] Table S1 shows that the average crystal size was calculated by using Scherrer's formula.

Furthermore, the chemical bonding of the synthesized material was confirmed by FT-IR spectroscopy. The peaks

https://doi.org/10.1021/acsomega.4c09437
ACS Omega 2025, 10, 1610−1623

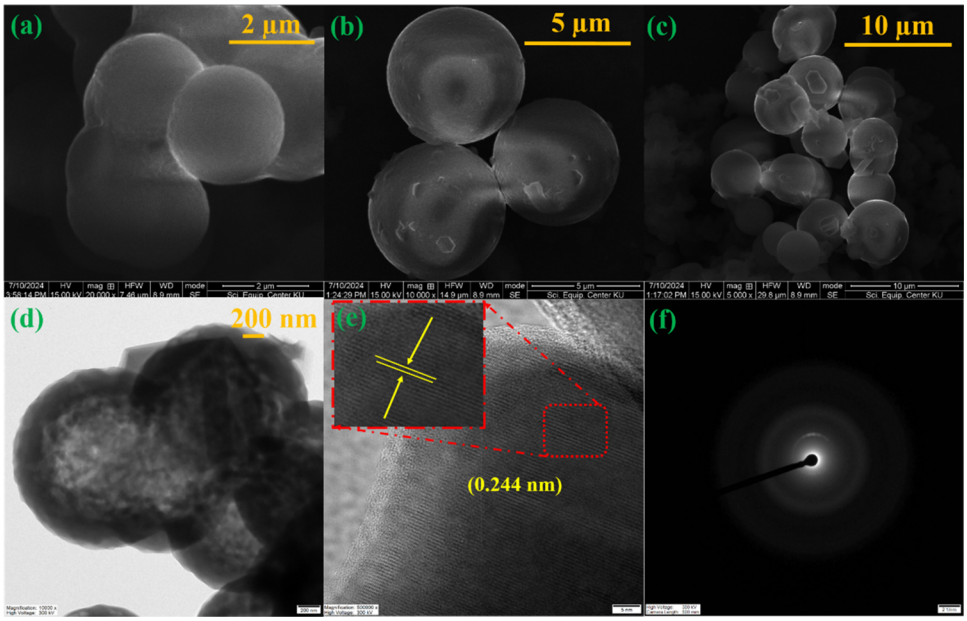

Figure 2. SEM (a–c), TEM (d), HR-TEM (e) images, and SAED pattern (f) of 3D Ni-TMAF.

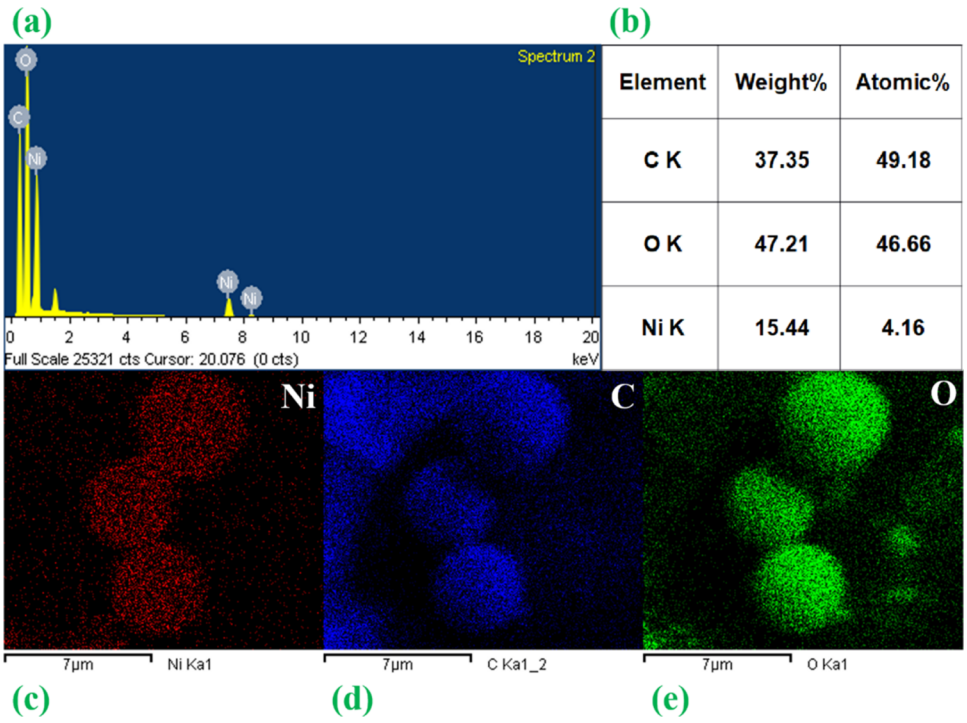

Figure 3. EDX spectra (a), elemental percentage (b), and mapping for 3D Ni-TMAF (c–e).

exhibited in N–H and O–H stretching vibration modes from 3000 to 3500 cm^{-1} at 3D Ni-TMAF. The asymmetric and symmetric stretching vibrations of carboxylic acid groups (C═O and C–O) appeared from 1570 to 1630 and from 1375 to 1433 cm^{-1} due to their interaction with Ni metal ions.[38] Furthermore, Figure 1b shows that the 1108 cm^{-1} band corresponds to the C–N vibrational frequencies, which indicates the coordination of Ni metal ions with DMF molecules. The bands at 869 and 945 cm^{-1} exhibit C–C stretching and C–H ring-out-of-plane vibrations of TMA, respectively.[39,40] Importantly, the bands from 430 to 777 cm^{-1} were related to metal–oxygen vibrations (Ni–O bonds). The results confirmed that the TMA was chelated with Ni ionic species and generated the 3D Ni-TMAF.

The more detailed characterization and the morphological traits of the as-prepared material were obtained from SEM and TEM analysis. In Figure 2a–d, the SEM and TEM pictures of 3D Ni-TMAF display a very clear sphere-like structure. These studies demonstrate how metals on TMA linkers altered the dimensions and morphologies of 3D Ni-TMAF. A high dispersion of 3D Ni-TMAF is observed in Figure 2e. The value of lattice fringes was determined as 0.244 nm, corresponding to the ascription of the crystalline plane of the central metal of nickel.[41] Furthermore, the selected area

https://doi.org/10.1021/acsomega.4c09437
ACS Omega 2025, 10, 1610–1623

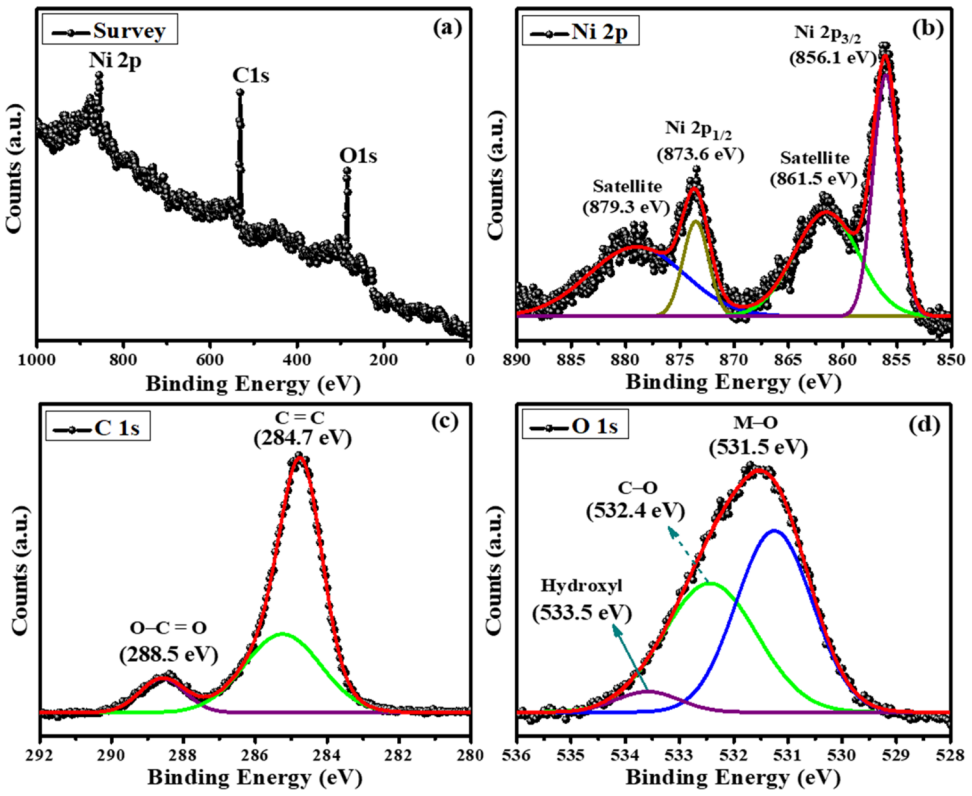

Figure 4. XPS of 3D Ni-TMAF: (a) survey, (b) Ni 2p, (c) C 1s, and (d) O 1s.

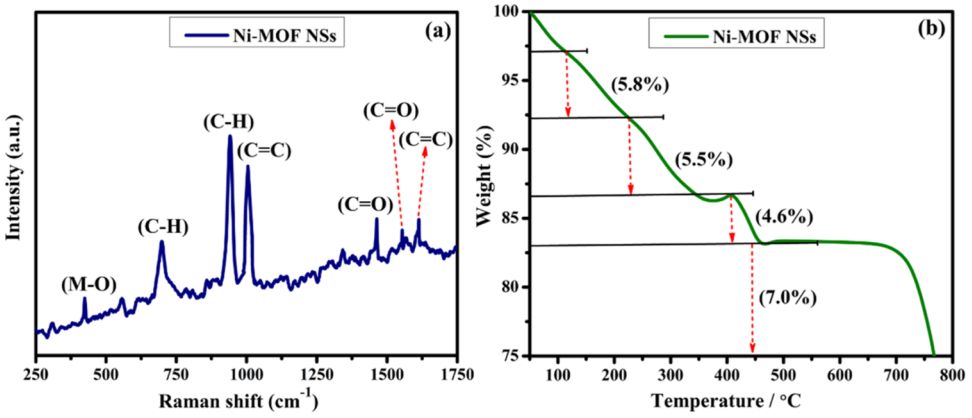

Figure 5. Raman spectroscopy (a) and TGA (b) for 3D Ni-TMAF.

electron diffraction (SAED) pattern of 3D Ni-TMAF appears with an elevated degree of crystallinity (Figure 2f). Further, the energy-dispersive X-ray (EDX) spectra of 3D Ni-TMAF (Nickel (Ni), Carbon (C), and Oxygen (O)) are shown in Figure 3a. Moreover, the elemental percentage of the as-prepared material is shown in Figure 3b. In addition, the elemental mapping also evaluates the presence of suitable elements (Ni, C, and O) on the surface of the material, as presented in Figure 3c−e.

The elemental composition and chemical state of 3D Ni-TMAF were determined using the XPS technique. In Figure 4a, the typical peaks in the survey spectrum indicated the presence of Ni, C, and O in 3D Ni-TMAF, which was evidenced from the high-resolution XPS spectra of Ni 2p, C 1s, and O 1s. Figure 4b reveals that the peaks at 856.1 and 873.6 eV with a spin-energy difference of 17.5 eV were connected with Ni $2p_{3/2}$ and Ni $2p_{1/2}$, as well as the broad bands at 861.5 and 879.3 eV were related to the shakeup satellite peaks of Ni $2p_{3/2}$ and Ni $2p_{1/2}$.[42] In Figure 4c, the peaks at 284.7 and 288.5 eV were created by the aromatic-related carbon−carbon double bond (C═C) and the carboxylate group (O−C═O) bonds, respectively.[43] Figure 4d shows three suited peaks at 533.5, 532.4, and 531.5 eV, which correspond to oxygen in surface hydroxyl, C−O, and metal−oxygen (M−O). This analysis confirmed that the TMA organic linker was effectively chelated into the Ni ion.

In addition, Figure 5a depicts the Raman spectra of 3D Ni-TMAF. The peak at 422 cm^{-1} matches the characteristic peak of M−O (M: Ni^{2+}) in Ni-TMAF. The peaks at 699 and 942 cm^{-1} matched with bending vibrations and bending modes of out-of-plane (C−H). The peaks at 1005 and 1612 cm^{-1} correspond to stretching modes of the C═C bond found in

https://doi.org/10.1021/acsomega.4c09437
ACS Omega 2025, 10, 1610−1623

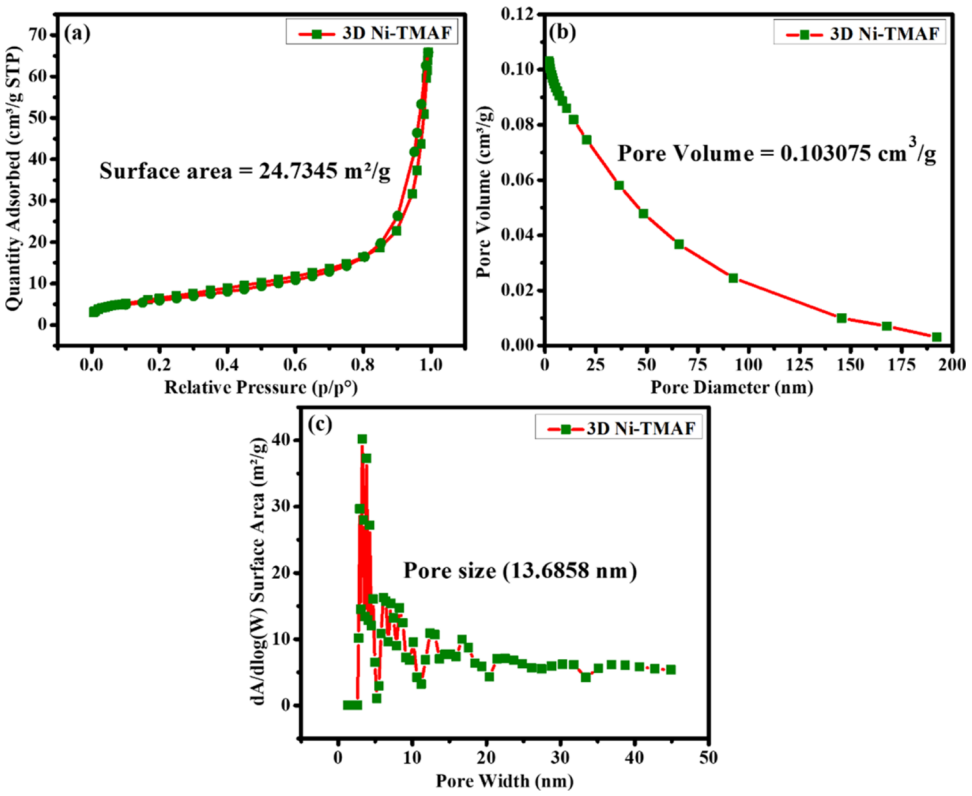

Figure 6. BET analysis of 3D Ni-TMAF: (a) surface area, (b) pore volume, and (c) pore size of 3D Ni-TMAF.

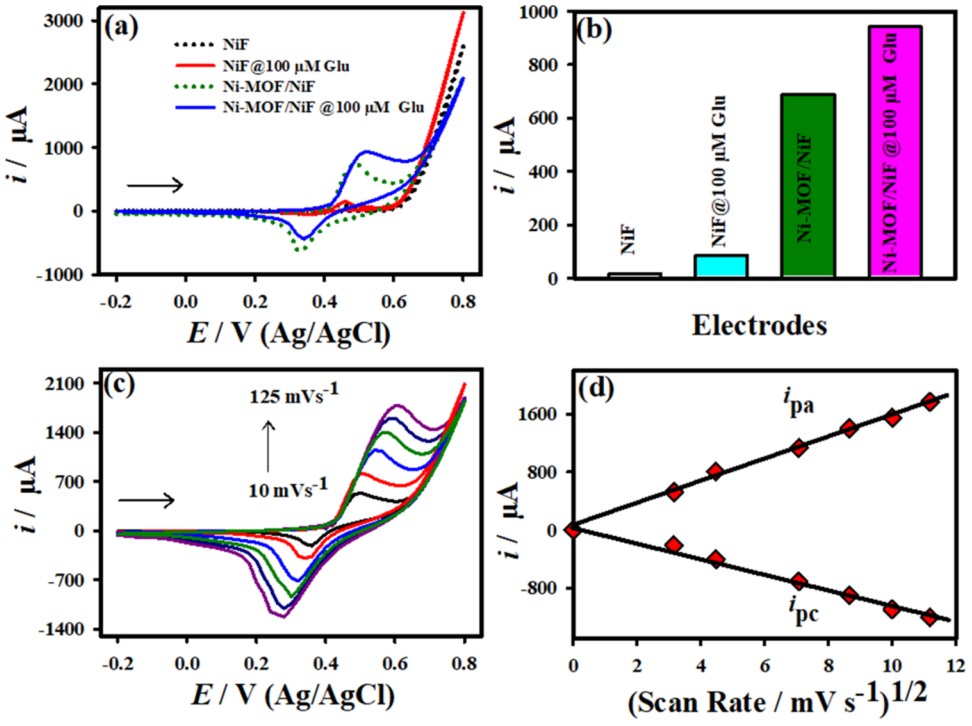

Figure 7. (a) CV curves of NF and Ni-TMAF/NF electrodes without glucose (dotted line) and with 100 μM glucose recorded at the scan rate of 20 mV s^{-1}. (b) Corresponding oxidation current response of various electrodes of NF and Ni-TMAF/NF. (c) CV curves of the Ni-TMAF/NF electrode with 100 μM of glucose recorded at different scan rates; (d) plot of anodic and cathodic currents against the square root of scan rates for Ni-TMAF/NF with 100 μM of glucose (electrolyte: 1.0 M NaOH).

the aromatic organic linker.[44] Additionally, the carboxylate units of TMA exhibit symmetric and asymmetric stretching of C═O at 1464 and 1554 cm^{-1}, respectively. Furthermore, the thermogravimetric analysis (TGA) curve of 3D Ni-TMAF is shown in Figure 5b. Particularly, the removal of DMF and H_2O adsorbed over the surface of the 3D Ni-TMAF was the main

https://doi.org/10.1021/acsomega.4c09437
ACS Omega 2025, 10, 1610−1623

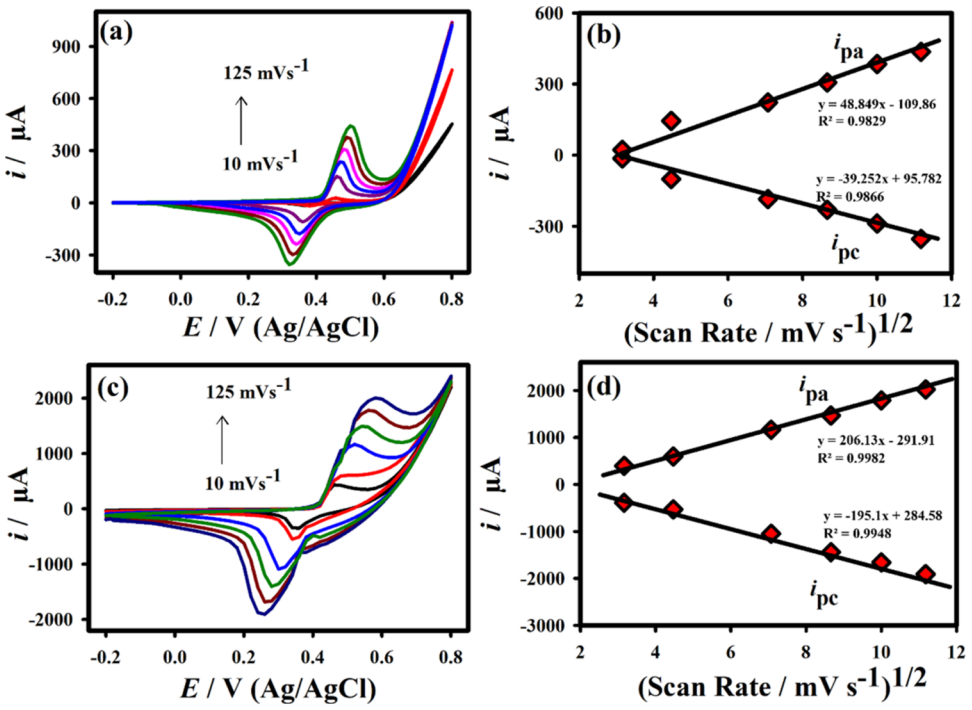

Figure 8. CV curves of NF (a) and Ni-TMAF/NF (c) electrode recorded at various scan rates from 10−125 mV s^{-1}. The corresponding plot of anodic and cathodic currents against the square root of scan rates for NF and Ni-TMAF/NF electrode (b, d). Electrolyte: 1.0 M NaOH.

cause of the initial weight loss, which was obtained between 115 and 225 °C. The other two weight loss curves of the area were detected at temperatures between 405 and 465 °C and up to 500 °C. These are ascribed to the decay of the organic linker and the remaining chemical components, respectively, which leads to the conversion into metal oxide. Consequently, these results showed that the 3D Ni-TMAF had virtuous thermal stability up to around 405 °C, after which the organic framework began to decompose significantly. The conversion of the Ni-MOF to NiO was confirmed by the final residue at high temperatures. The overall results of the prepared 3D Ni-TMAF were well-characterized by scientific techniques such as XRD, FT-IR, FE-SEM, TEM, EDX, XPS, Raman, TGA, and BET.

Moreover, the surface area, pore volume, and pore size of 3D Ni-TMAF were measured by N_2 adsorption/desorption isotherms. Based on Brunauer−Emmett−Teller (BET) tests, 3D Ni-TMAF exhibits a surface area of 24.7345 m^2/g (Figure 6a). This larger surface space offers good electrochemical active catalytic performance for glucose sensors. Also, 3D Ni-TMAF with an enormous surface area demonstrates increased structural stability. This can result in longer oxidation lifetimes and stable functionality under numerous environmental circumstances. The Barrett−Joyner−Halenda (BJH) technique was employed to find the pore volume (0.103075 cm^3/g) and pore size (13.6858 nm) of 3D Ni-TMAF, as displayed in Figure 6b,c. Also, the small widths of the pore size distribution points indicate that the mesoporous substances are homogeneous in shape. Hence, it significantly improves the diffusion of reacting substances throughout the material, leading to a more effective catalysis.

3.2. Electrocatalytic Measurements of NiF/Ni-TMAF. The developed Ni-TMAF/NF electrode's electrocatalytic activity was evaluated by testing its ability to oxidize glucose. The electrochemical behavior of the bare NF and Ni-TMAF/NF electrodes is compared in the cyclic voltammetry (CV) curves shown in Figure 7a in the presence (solid curve) and absence (dotted curve) of 100.0 μM glucose. These curves were captured between −0.2 and 0.8 V versus Ag/AgCl at a scan rate of 20 mV s^{-1}. In this configuration, investigating the electrocatalytic oxidation at the modified electrodes plays an essential component, enabling its rapid sensing toward glucose. Figure 7a displays that the anodic peak current (i_a) increased by approximately 941.79 μA at a potential of 0.52 V after the prior addition of glucose (100.0 μM). This increase in anodic current is attributed to the electrochemical detection of glucose, indicating enhanced electrocatalytic activity of the Ni-TMAF/NF electrode toward robust glucose sensing ability. In contrast to the Ni-TMAF/NF electrode, the bare NF electrode did not show a significant enhancement in anodic current in the presence of glucose, as demonstrated in Figure 7a. This suggests that the bare NiF electrode exhibits minimal electrocatalytic activity for glucose oxidation, highlighting the improved extreme performance of the Ni-TMAF/NF electrode, which is shown in Figure 7b. Figure 7c displays the cyclic voltammetry (CV) curves of the Ni-TMAF/NF electrode, recorded at various scan rates from 10−125 mV s^{-1} in the presence of 100.0 μM glucose. These CV curves likely provide insight into the relationship between the scan rate and the electrode's electrochemical behavior, particularly in terms of current response and kinetics of glucose oxidation. Figure 7d depicts the observation of a linear plot when anodic (i_{pa}) and cathodic (i_{pc}) peak currents are plotted against the square root of the scan rates, suggesting that the electrochemical oxidation of glucose at the Ni-TMAF/NF electrode is a diffusion-controlled process. This linear relationship indicates that the reaction kinetics are influenced by the diffusion of glucose molecules to the electrode's exterior surface. This indicates that the glucose oxidation process is primarily governed by the diffusion of glucose molecules toward the

https://doi.org/10.1021/acsomega.4c09437
ACS Omega 2025, 10, 1610−1623

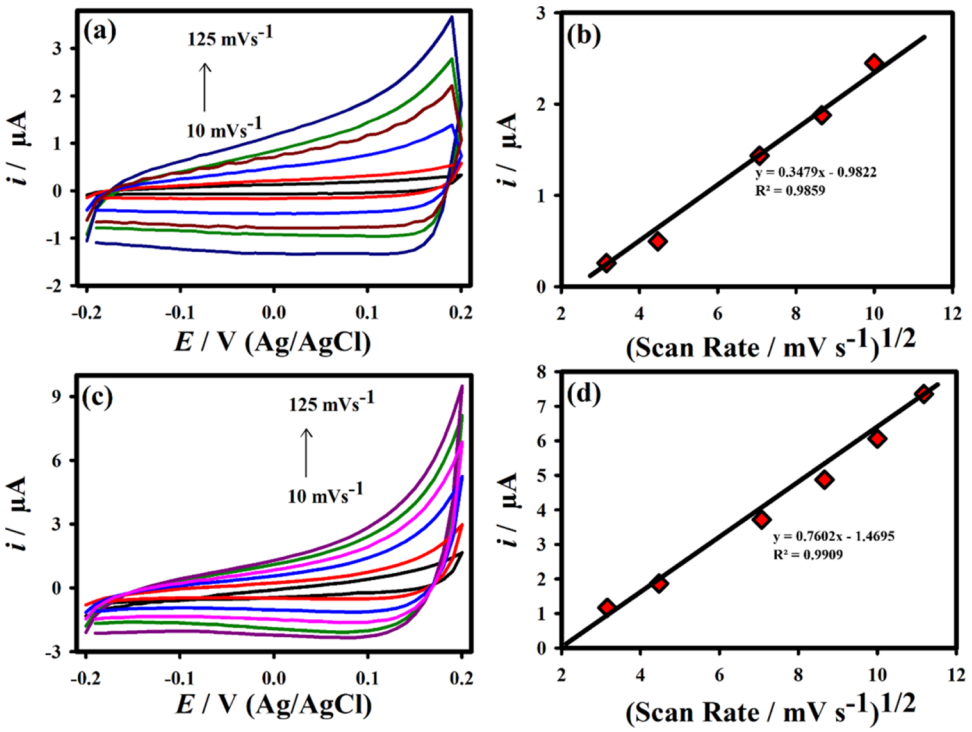

Figure 9. CV curves of NF (a) and Ni-TMAF/NF (c) electrodes recorded at the non-faradic region at various scan rates from 10−125 mV s^{-1}. The corresponding plot of anodic and cathodic currents against the square root of scan rates for NF and Ni-TMAF/NF electrodes (b, d). Electrolyte: 1.0 M NaOH.

electrode surface, which impacts the electrode's performance in the rapid detection of glucose. Nickel exhibits strong redox behavior, particularly in alkaline environments, where Ni^{2+}/Ni^{3+} transition plays a crucial role in glucose oxidation.[10] The observation that the electrochemical oxidation of glucose at the Ni-TMAF/NF electrode is an irreversible process indicates that the reaction does not easily reverse under the experimental conditions investigated in eqs 1 and 2.[10] This irreversibility can be attributed to the nature of the electrochemical reaction, which may involve complex redox processes or significant changes in the oxidation state of the glucose molecules. In the Ni-TMAF, the central metal atom of Nickel in the form of nickel hydroxide $Ni(OH)_2$ in Ni^{2+} has been oxidized in Ni(OOH) in Ni^{3+}, and the introduced glucose can get oxidized to give gluconolactone rapidly. This irreversibility might affect the stability and reproducibility of the sensor.[45,46] In addition, to optimize the constant applied potential, the varied applied potentials of 0.48, 0.50, and 0.52 were applied on the Ni-TMAF|NF electrodes toward the amperometric detection of glucose investigated in Figure S1. The constant applied potentials were chosen based on the preliminary catalytic studies toward the oxidation of glucose from cyclic voltammetry techniques.

$$Ni^{2+} \rightarrow Ni^{3+} + e^{-} \quad (1)$$

$$Ni^{3+} + \text{glucose} \rightarrow Ni^{2+} + \text{gluconolactone} \quad (2)$$

3.3. Electrochemical Redox Characteristics of NiF and Ni-TMAF/NF. The electrochemical redox properties of nickel foam (NF) incorporated into Ni-TMAF can be effectively studied using cyclic voltammetry (CV) under an alkaline medium of 0.1 M NaOH. This technique provides valuable insights into the electrochemical behavior of the material, specifically its redox processes, electrochemical active surface area, and electrocatalytic activity toward glucose. The electrode materials insights can be analyzed by cyclic voltammetry study of NF and Ni-TMAF/NF with anodic (i_{pa}) and cathodic (i_{pc}) current responses, and the square root of the scan rate relationship is displayed in Figure 8. The square root of the scan rate relationship indicates that the current response follows a diffusion-controlled electrochemical process where both anodic and cathodic currents (i_{pa} and i_{pc}) increase linearly with the square root of the scan rate ($\nu^{1/2}$). This linear relationship, typically shown in Figure 8a,c, the cyclic voltammograms, confirms that the redox reactions at the NF and Ni-TMAF/NF nanosphere electrodes are diffusion-controlled rather than a surface-controlled electrode process. The increase in the anodic oxidation current with increasing scan rates (from 10 to 125 mV s^{-1}) indeed demonstrates the linear dependence of the anodic peak current (i_{pa}) on the square root of the scan rate ($\nu^{1/2}$). This behavior is characteristic of a diffusion-controlled process, where the rate of electron transfer is governed by the diffusion of electroactive species to the electrode surface. As the scan rate increases, more electroactive species have less time to diffuse, resulting in higher current responses due to the faster rate of electron transfer. From the linear plot between anodic peak current (i_{pa}) and the square root of scan rate ($\nu^{1/2}$), we get $R^2 = 0.99$, which signifies that the kinetics of the redox reaction are predominantly controlled by diffusion rather than adsorption or surface processes shown in Figure 8b,d. This finding supports the electrocatalytic activity of the Ni-TMAF/NF electrode, as the material facilitates efficient electron transfer during the oxidation process, making it a promising candidate for applications such as sensing, where rapid and consistent current responses are essential.

Rather than estimating the geometric surface area of the electrode, the electrochemical active surface area (ECASA)

https://doi.org/10.1021/acsomega.4c09437
ACS Omega 2025, 10, 1610−1623

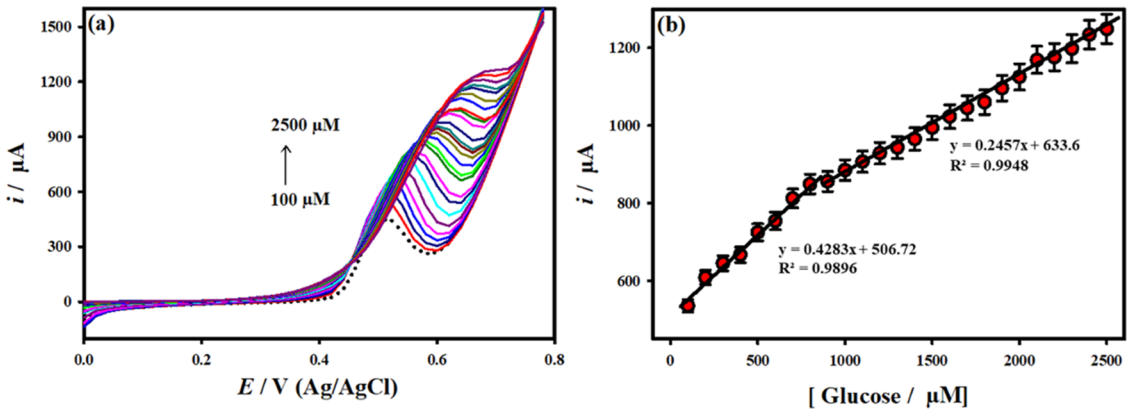

Figure 10. (a) LSV curves of Ni-TMAF/NF electrode with glucose at various concentrations of glucose recorded at the scan rate of 20 mV s^{-1}. (b) Corresponding oxidation current response against the concentration of glucose. Electrolyte: 1.0 M NaOH.

Table 1. List of Reported Electrochemical Sensors with the Present Sensor Based on Ni-TMAF/NF toward Glucose Sensing

electrode	technique	sensitivity	linear range (μM)	LOD [nM]	refs
Ni-MOF/CNTs	amperometry	13.85 mA mM^{-1} cm^{-2}	1 μM to 1.6 mM	0.82 μM	47
NC-MOFs/CCFs	amperometry	105.2 μA mM^{-1} cm^{-2}	0.04−3.13 mM	0.116 μM	48
		23 μA mM^{-1} cm^{-2}	3.63−8.28 mM		
CTGU-31/GCE	amperometry	2.198 μA μM^{-1} cm^{-2}	10−4000 μM	0.09 μM	49
Co-MOF/CC	amperometry		0.8−16 mM	0.15 mM	50
Ni-HHTT	amperometry	10,200 μA mM^{-1} cm^{-2}	0.5−4100 μM	0.15 μM	51
Cu-MOF/CNHs/GCE	amperometry		250 nM to 1.2 mM	78 nM	52
Zn-MOF/MWCNTs	amperometry	34.64 μA mM^{-1} cm^{-2}	0.020−8.14 mM	0.037 mM	53
Cu-MOF/GCE	amperometry	89 μA mM^{-1} cm^{-2}	0.06−5000 μM	0.01 μM	54
Ni-TMAF/NF	amperometry	203.89 μA μM^{-1} cm^{-2}	10−230 μM	0.33 μM	this work
	LSV	26.76 μA μM^{-1} cm^{-2}	100−800 μM		
		15.36 μA μM^{-1} cm^{-2}	900 μM to 2.5 mM		

provides an estimate of the actual surface area that is the electrochemically active site for reaction. The catalytic performance of the electrode is improved by having more active sites, which is often indicated by a higher ECASA value shown in Figure 9. By calculating C_{dl} from these CV curves and dividing it by the specific capacitance C_s, which is approximately 0.04 mF cm^{-2} for a smooth surface, the ECASA is determined.[41] This value provides insight into the effectiveness of the electrode material in providing accessible active sites for electrochemical reactions. These measurements are typically performed in a non-faradic potential range (i.e., where no significant faradaic reactions occur) to evaluate the capacitive behavior of the electrode investigated in Figure 9a,c. The resulting current is primarily due to the charging and discharging of the double layer at the electrode−electrolyte interface. The double layer capacitance (C_{dl}) can be calculated from Figure 9b,d for the NF and Ni-TMAF modified NF, respectively. The electrochemical active surface area (ECSA) values for the bare nickel foam (NF) and Ni-TMAF/NF modified electrodes were estimated to be approximately 0.0037 and 0.0486 cm^{-2}, respectively. The significantly higher ECASA value of 0.0486 cm^{-2} for the Ni-TMAF/NF modified electrode suggests that the modification with Ni-TMAF drastically increased the active surface area approximately 13.13 times higher when compared to unmodified NF. This enhancement provides more active sites for electrochemical reactions, which can contribute to better catalytic performance and higher current densities during operation. The nanostructured features (Ni-TMAF on NF) can lead to a synergistic effect, improving the material's electric and ionic conductivity, electron transfer rate, and overall electrochemical response. The incorporation of Ni-TMAF enhances the electrochemical performance due to the increased surface area and more active sites for redox reactions. For instance, an incredibly sensitive and important technique for examining the interfacial properties of electrochemical sensing platforms in modified electrodes is electrochemical impedance spectroscopy (EIS), which offers built-in information on the conductance, resistance, and capacitance at the electrode−electrolyte interface. After modification, Ni-TMAF gives high conductivity. Reducing the R_{ct} value of Ni-TMAF improves the intrinsic properties of ionic and electronic properties of materials. The fitted electronic equivalent circuit is shown in Figure S2. The Nyquist plot of the Ni-TMAF on NF exhibited a smaller polarization resistance (R_p) of ∼402 Ω·cm^2 and a high capacitance value in comparison to the bare NF electrode (∼485 Ω·cm^2). This result indicates that the Ni-TMAF on NF electrodes facilitates fast electron transfer kinetics at the interface.

3.4. Electrochemical Detection of Enzyme-Mimic Glucose Sensors. Figure 10a displays the linear sweep voltammetry (LSV) curve of the Ni-TMAF/NF nanospheres upon adding various concentrations of glucose, starting from 100 μM to 2.5 mM in 0.1 M NaOH. The anodic current increased quickly and extended at moving to a slightly positive potential for robust oxidation of glucose in the increasing concentrations. Figure 10b displays the calibration plot of oxidative anodic current, revealing a linear relationship to glucose concentration. In short, two linear lines were obtained for the Ni-TMAF/NF electrodes upon the addition of glucose

https://doi.org/10.1021/acsomega.4c09437
ACS Omega 2025, 10, 1610−1623

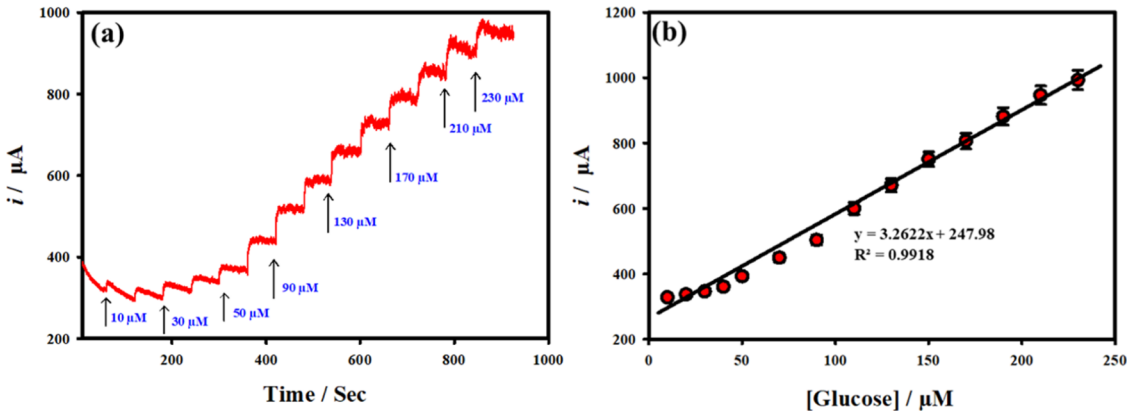

Figure 11. (a) Chronoamperometry (i–t) curves of the Ni-TMAF/NF electrode with glucose at various concentrations of glucose recorded at applied potential E_{app} 0.52 V. (b) Corresponding oxidation current response against concentration of glucose in alkaline 1.0 M NaOH.

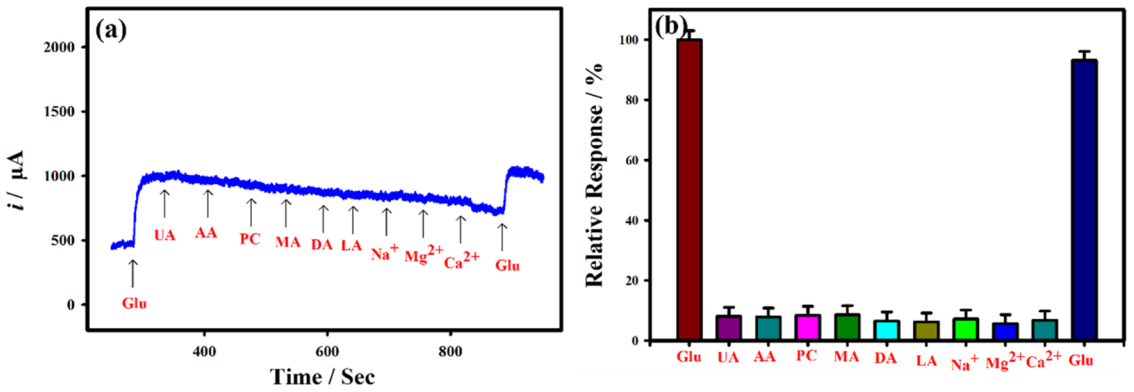

Figure 12. (a) CA i–t curve of the Ni-TMAF/NF electrode detected in 1.0 M NaOH with the presence of 10 μM glucose, 0.1 mM UA, 0.1 mM AA, 0.1 mM PC, 0.1 mM MA, 0.1 mM DA, 0.1 mM LA, 0.1 mM Na^+, 0.1 mM Mg^{2+}, 1.0 mM Ca^{2+}, and 10 μM glucose at E_{app}: 0.52 V. (b) Measured relative response of the Ni-TMAF/NF electrode in the presence of different interferences.

with different concentrations, starting from 100 to 800 μM (correlation coefficient of R^2 = 0.989) with a sensitivity of 26.76 μA μM^{-1} cm^{-2}, and 900 μM to 2.5 mM (R^2 = 0.994) with a sensitivity of 15.36 μA μM^{-1} cm^{-2}. Due to a rise in the small concentration of glucose diffusion and high catalytic behavior, the Ni-TMAF/NF electrodes revealed high sensitivity (26.76 μA μM^{-1} cm^{-2}) in less concentration of glucose. The catalytic behavior of the Ni-TMAF/NF electrodes may be impacted by glucose due to the adsorbed oxidized substances at the electrode, providing less sensitivity (15.36 μA μM^{-1} cm^{-2}). Hence, this sensor provided dual linear lines for the sensing of glucose. Furthermore, the limit of detection was determined as 5.55 μM using $3s/b$, where "s" indicates the standard deviation of the blank and "b" represents the slope. As displayed in Table 1, the Ni-TMAF/NF electrode-based sensing technique outperformed previously reported glucose sensors in terms of detection limit, sensitivity, and linear range.

In addition, Figure 11a reveals that the chronoamperometric (i–t) response of the Ni-TMAF/NF electrode was recorded during the sequential addition of glucose at 60 s intervals. This was performed at an applied electrode potential (E_{app}) of 0.60 V vs Ag/AgCl. The response curve showed distinct, sharp current increases upon each glucose addition, indicating the electrode's high sensitivity toward glucose. This consistent rise in current corresponds to the oxidation of glucose at the Ni-TMAF/NF surface, and the steady-state current is achieved within seconds after each addition. The behavior highlights the electrode's efficiency and rapid responsiveness toward glucose detection. The applied potential of 0.52 V vs Ag/AgCl was selected based on the maximum electrocatalytic glucose oxidation peak potential observed during earlier cyclic voltammetry (CV) studies. This potential corresponds to the most efficient glucose oxidation at the Ni-TMAF/NF electrode surface, where the current response is maximized due to the enhanced electrocatalytic activity of the Ni-based nanomaterial. By choosing this optimal potential, the sensor ensures a strong and stable current response for glucose detection, minimizing interference and maximizing sensitivity during the chronoamperometric (i–t) measurements. The anodic catalytic current was increased steadily after the addition of different concentrations of glucose, ranging from 10.0 to 230 μM, as shown in Figure 11a. Figure 11b displays the corresponding calibration plot of Figure 11a. At an applied potential of 0.52 V vs Ag/AgCl, a linear relationship was achieved between the anodic currents and the glucose concentration in the range of 10.0 to 230.0 μM. This linearity was confirmed with a high correlation coefficient of R^2 = 0.9918, indicating excellent accuracy and consistency in the sensor's response across this concentration range. The sensor demonstrated a sensitivity of approximately 203.89 μA μM^{-1} cm^{-2}, highlighting its strong electrocatalytic performance for glucose oxidation. This high sensitivity ensures that even low concentrations of glucose can be reliably detected, making the Ni-TMAF/NF electrode a promising candidate for practical glucose sensing applications. When increasing glucose concentration ranges could be linked to oxidized glucose

https://doi.org/10.1021/acsomega.4c09437
ACS Omega 2025, 10, 1610−1623

species rapidly to the Ni-TMAF/NF electrode surface, in terms of glucose detection, the limit of detection (LOD) was discovered to be 0.33 μM. To the best of our knowledge, the current Ni-TMAF/NF-based sensor for glucose detection has a wide linear range, a high sensitivity, and a lower detection limit.

3.5. Selectivity of the Glucose Sensor. Moreover, Ni-TMAF nanospheres offer high stability and resistance to common interferences such as ascorbic acid, uric acid, and dopamine, which often hinder glucose detection in biological samples. To evaluate the selectivity of the Ni-TMAF/NF electrode for glucose sensing, amperometry measurements were conducted in the presence of various potential interfering species. These interferents were tested at concentrations approximately 10 times higher than those of glucose. Despite the elevated levels of interferents, the Ni-TMAF/NF sensor maintained a stable performance, demonstrating its excellent selectivity for glucose detection even in complex mixtures. This suggests that the sensor effectively discriminates against common electroactive species, making it highly suitable for practical applications, such as glucose monitoring in biological samples. Figure 12a displays the $i-t$ curve of the Ni-TMAF/NF electrode toward the 10.0 μM glucose in the absence and the presence of 0.1 mM uric acid (UA), 0.1 mM ascorbic acid (AA), 0.1 mM paracetamol (PA), 0.1 mM maltose (MA), 0.1 mM dopamine (DA), 0.1 mM lactose (LA), 0.1 mM Mg^{2+}, 0.1 mM Na^{+}, and 0.1 mM Ca^{2+}. The relative amperometric current was plotted in terms of glucose oxidation and is shown in Figure 12b. The Ni-TMAF/NF electrode exhibited remarkable retention of its electrocatalytic activity for glucose electrooxidation, maintaining approximately 96% of its performance even in the presence of a mixture of potential interferences. This strong resilience against interference further highlights the sensor's exceptional selectivity and reliability for glucose detection, ensuring minimal signal loss when dealing with complex sample environments. The Ni-TMAF/NF electrode demonstrated excellent selectivity for glucose detection, as potential electroactive interferents, including uric acid, ascorbic acid, paracetamol, maltose, dopamine, lactose, and others, showed no significant interactions with the Ni-TMAF/NF nanomaterials. Despite the presence of these common interfering molecules, the sensor maintained its high electrocatalytic activity, ensuring a reliable glucose measurement without being affected by the electrochemical signals of these substances. This further supports the sensor's robustness in complex sample matrices, making it suitable for practical applications in clinical or biomedical settings. In contrast to other active molecules, the as-developed Ni-TMAF/NF electrode provided a more practical environment for the adsorption and oxidation of glucose. According to this suggestion, the manufactured Ni-TMAF/NF electrode showed respectable selectivity to the glucose.

3.6. Durability of the Glucose Sensor. The observation in Figure 13 shows that the catalytic anodic current density of the Ni-TMAF/NF electrode decreased by only approximately 11% during glucose oxidation after continuous measurements for over 5000 s. This comparatively small reduction indicates that the sensor can continue to function for extended glucose detection applications due to its high durability and stability. The inset Figure 13 shows CV cycles of before and after durability there is no substantial decrease in the anodic current can provide information on the stability of the Ni-TMAF/NF. Stable peak currents over 5000 s indicate good durability and

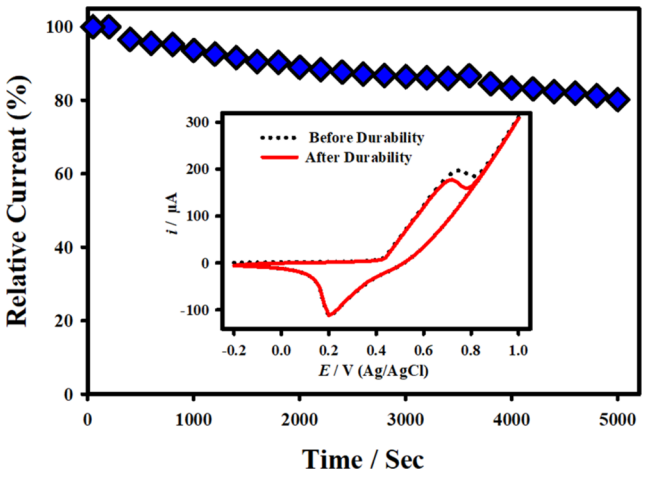

Figure 13. Chronoamperometric responses obtained for the Ni-TMAF|NF in 100 μM glucose +0.1 M NaOH for 5000 s (E_{app}: 0.52 V). Inset: CV curves for the Ni-TMAF|NF before (dotted) and after (solid) durability analysis.

electrochemical stability, which are essential for long-term practical applications.

3.7. Practical Application in Human Sweat and Saliva Samples. Additionally, the practical applicability of glucose detection in human sweat and saliva samples was tested using the current Ni-TMAF|NF sensing electrode. As mentioned in Section 2, the real sweat and saliva samples were prepared and then diluted approximately 100 times using a 1.0 M NaOH solution. Using this technique, the baseline level of glucose for the recovery requirements for glucose levels of 5.0 to 20.0 μM was determined in both sweat and saliva samples before glucose was added. The rapid and steady-state current response after each glucose addition indicates that the Ni-TMAF/NF sensing electrode exhibits quick and stable electrocatalytic activity. This is an important feature for real-time glucose monitoring as it shows that the sensor can reliably detect varying glucose levels without significant delay or drift. Table 2 shows that the recovery rates of glucose detection in

Table 2. Evaluation of Real Samples Based on Recovery Tests of Glucose at the Ni-TMAF/NF Electrode for Real Samples (Sweat and Saliva) (n = 3)

electrode Ni-TMAF/NF	added (μM)	found (μM)	recovery (%)	RSD (%)
sweat	5	4.82	96.4	4.90
	10	9.81	98.1	2.31
	20	19.6	98.0	0.73
saliva	5	4.8	96	3.11
	10	9.72	97.2	1.89
	20	19.7	98.5	1.79

human sweat and saliva samples. Recovery rates are critical in assessing the accuracy of the sensor as they reflect how well the sensor can quantify glucose levels compared to known concentrations. The recovery values of the glucose in human sweat were raised about ~96.4−~98.1% with RSD% values in the range of 0.73−4.90. In human saliva samples, the recovery values were extended in the range 96.0 to 98.5%, with RSD% values between 1.79 and 3.11. The developed glucose sensor platform based on Ni-TMAF/NF nanomaterials shows strong potential for biomedical applications, likely due to its favorable

https://doi.org/10.1021/acsomega.4c09437
ACS Omega 2025, 10, 1610−1623

attributes such as high sensitivity, rapid response, and accurate recovery rates in real biological samples such as serum and sweat. This positions the sensor as a promising tool for noninvasive glucose monitoring in clinical diagnostics.

4. CONCLUSIONS

The study successfully demonstrated a small electrochemical sensing platform for glucose detection. The developed sensors exhibit promising characteristics, including high sensitivity, a wide linear detection range, rapid response times, and excellent selectivity. The Ni-TMAF electrodes exhibited outstanding electrocatalytic oxidation properties and demonstrated the capability of detecting glucose even at very small concentrations. This high sensitivity, combined with the electrodes' wide linear detection range, makes them particularly effective for glucose sensing, allowing for precise detection even at low glucose levels, which is crucial for accurate monitoring in both clinical and physiological environments. This can be attributed to the abundant electrochemical surface area (ECSA), boosted charge transfer efficiency, and well-dispersed 3D Ni-TMAF-based electrochemical sensors revealing swift detecting response time, a low limit of detection, greater sensitivity with a wide range, outstanding reproducibility, and a strong ability to sensing of glucose.

■ ASSOCIATED CONTENT

Supporting Information

The Supporting Information is available free of charge at https://pubs.acs.org/doi/10.1021/acsomega.4c09437.

Average crystal size of 3D Ni-TMAF; chronoamperometric $i-t$ curves of the Ni-TMAF on NF recorded in the absence (dotted curve) and presence (solid curve) of 100 μM glucose in 1.0 M NaOH at various applied potentials (E_{app}), and Nyquist plots of EIS for Ni Foam (red) and Ni-TMAF on NF (blue) (PDF)

■ AUTHOR INFORMATION

Corresponding Author

Sirikanjana Thongmee − *Department of Physics, Faculty of Science, Kasetsart University, Bangkok 10900, Thailand;* orcid.org/0000-0001-8294-9997; Phone: +66 86 999-3234; Email: fscisjn@ku.ac.th

Authors

Rajaji Pavadai − *Department of Chemistry, Faculty of Science, Kasetsart University, Bangkok 10900, Thailand; Department of Chemistry, Dhanalakshmi Srinivasan College of Engineering and Technology, Chennai 603104, India;* orcid.org/0009-0003-3233-9455

Mani Arivazhagan − *Research Laboratory for Analytical Instrument and Electrochemistry Innovation, Department of Chemistry, Faculty of Science, Chiang Mai University, Chiang Mai 50200, Thailand*

Jaroon Jakmunee − *Research Laboratory on Advanced Materials for Sensor and Biosensor Innovation, Materials Science Research Center, and Center of Excellence for Innovation in Chemistry, Faculty of Science, Chiang Mai University, Chiang Mai 50200, Thailand;* orcid.org/0000-0001-7522-0727

Nethaji Pavadai − *Department of Materials Science, Faculty of Science, Chulalongkorn University, Bangkok 10330, Thailand*

Revathi Palanisamy − *Department of Materials Science, Faculty of Science, Chulalongkorn University, Bangkok 10330, Thailand*

Ganesha Honnu − *Department of Physics, Faculty of Science, Kasetsart University, Bangkok 10900, Thailand;* orcid.org/0000-0002-5622-7517

Sutasinee Kityakarn − *Department of Chemistry, Faculty of Science, Kasetsart University, Bangkok 10900, Thailand*

Jeerawan Khumphon − *Department of Physics, Faculty of Science, Kasetsart University, Bangkok 10900, Thailand*

Chaisak Issro − *Department of Physics, Faculty of Science, Burapha University, Chonburi 20131, Thailand*

Dusadee Khamboonrueang − *Faculty of Science and Technology, Nakhon Sawan Rajabaht University, Nakhon Sawan 60000, Thailand*

Complete contact information is available at: https://pubs.acs.org/10.1021/acsomega.4c09437

Author Contributions

R.P.: Writing—original draft, validation, methodology, investigation, data curation, and conceptualization. A.M.: Writing—review and editing and formal analysis. J.J.: Formal analysis. N.P.: Formal analysis. R.P.: Formal analysis. G.H.: Formal analysis. S.K.: Writing—review and editing and supervision. J.K.: Formal analysis. C.I.: Formal analysis. D.K.: Formal analysis. S.T.: Writing—review and editing, supervision, project administration, and funding acquisition.

Notes

The authors declare no competing financial interest.

■ ACKNOWLEDGMENTS

This research has received funding support from the National Science, Research and Innovation Fund (NSRF) via the Program Management Unit for Human Resources & Institutional Development, Research and Innovation (grant number: B13F670067). The authors wish to acknowledge the financial support provided by the National Research Council of Thailand (NRCT) and Kasetsart University for funding (N42A650277), Thailand. Moreover, this research has received funding support from the NSRF via the Program Management Unit for Human Resources & Institutional Development, Research and Innovation (grant number B05F640203).

■ REFERENCES

(1) Kim, K.; Kim, J.; Bae, Y. S. Zn-Co Bimetallic Zeolitic Imidazolate Frameworks as Nonenzymatic Electrochemical Glucose Sensors with Enhanced Sensitivity and Chemical Stability. *ACS Sustainable Chem. Eng.* **2022**, *10* (35), 11702−11709.

(2) Arivazhagan, M.; Mohan, B.; Jakmunee, J. Nanostructured Metallic Enzymes Mimic for Electrochemical Biosensing of Glucose. *Green Anal. Chem.* **2024**, *10*, No. 100127.

(3) Ashok, A.; Nguyen, T. K.; Barton, M.; Leitch, M.; Masud, M. K.; Park, H.; Truong, T. A.; Kaneti, Y. V.; Ta, H. T.; Li, X.; Liang, K.; Do, T. N.; Wang, C. H.; Nguyen, N. T.; Yamauchi, Y.; Phan, H. P. Flexible Nanoarchitectonics for Biosensing and Physiological Monitoring Applications. *Small* **2023**, *19* (9), No. 2204946.

(4) Zhou, F.; Wang, J.; Tang, Y.; Song, X.; Zhou, W.; Li, Y.; Gao, F. Enhanced Sensing Performance of Flexible Non-Enzymatic Electrochemical Glucose Sensors Using Hollow Fe3O4 Nanospheres of Controllable Morphologies. *Ceram. Int.* **2024**, *50* (20), 38009−38021.

(5) He, F.; Wang, H.; Du, P.; Li, T.; Wang, W.; Tan, T.; Liu, Y.; Ma, Y.; Wang, Y.; Abd El-Aty, A. M. Personal Glucose Meters Coupled with Signal Amplification Technologies for Quantitative Detection of

Non-Glucose Targets: Recent Progress and Challenges in Food Safety Hazards Analysis. *J. Pharm. Anal.* **2023**, *13* (3), 223−238.
(6) Babu, K. J.; kumar, T. R.; Yoo, D. J.; Phang, S.-M.; kumar, G. G. Electrodeposited Nickel Cobalt Sulfide Flowerlike Architectures on Disposable Cellulose Filter Paper for Enzyme-Free Glucose Sensor Applications. *ACS Sustainable Chem. Eng.* **2018**, *6* (12), 16982−16989.
(7) Jiang, H.; Xia, C.; Lin, J.; Garalleh, H. A. L.; Alalawi, A.; Pugazhendhi, A. Carbon Nanomaterials: A Growing Tool for the Diagnosis and Treatment of Diabetes Mellitus. *Environ. Res.* **2023**, *221*, No. 115250.
(8) Xie, Q.; Nie, M.; Zhang, F.; Shao, X.; Wang, J.; Song, J.; Wang, Y. An Unexpected Interaction between Diabetes and Cardiovascular Diseases on Cognitive Function: A Cross-Sectional Study. *J. Affective Disord.* **2024**, *354*, 688−693.
(9) Mohanapriya, D.; Satija, J.; Senthilkumar, S.; Ponnusamy, V. K.; Thenmozhi, K. Design and Engineering of 2D MXenes for Point-of-Care Electrochemical Detection of Bioactive Analytes and Environmental Pollutants. *Coord. Chem. Rev.* **2024**, *507*, No. 215746.
(10) kumar, T. R.; Babu, K. J.; Yoo, D. J.; Kim, A. R.; kumar, G. G. Binder Free and Free-Standing Electrospun Membrane Architecture for Sensitive and Selective Non-Enzymatic Glucose Sensors. *RSC Adv.* **2015**, *5* (52), 41457−41467.
(11) Teymourian, H.; Barfidokht, A.; Wang, J. Electrochemical Glucose Sensors in Diabetes Management: An Updated Review (2010−2020). *Chem. Soc. Rev.* **2020**, *49* (21), 7671−7709.
(12) Vasuki, K.; Siva, G.; Balasubramani, A.; Pannipara, M.; Al-Sehemi, A. G.; Xia, Y.; Fang, R.; Yoo, D. J.; Kumar, T. R.; Ramachandran, R.; kumar, G. G. Surfactant and Binder Free Hierarchical NCNPs@CuO Nanostructures on ITO for the Cost Effective Enzyme-Free Glucose Sensor Applications. *Appl. Phys. A* **2019**, *125* (6), No. 384.
(13) Tamilarasi, S.; Kumar, R. S.; Cho, K.-B.; Kim, C.-J.; Yoo, D. J. High-Performance Electrochemical Detection of Glucose in Human Blood Serum Using a Hierarchical NiO2 Nanostructure Supported on Phosphorus Doped Graphene. *Mater. Today Chem.* **2023**, *34*, No. 101765.
(14) Huang, Q.; Chen, J.; Zhao, Y.; Huang, J.; Liu, H. Advancements in Electrochemical Glucose Sensors. *Talanta* **2025**, *281*, No. 126897.
(15) Boakye, A.; Yu, K.; Chai, H.; Xu, T.; Houston, L. S.; Asinyo, B. K.; Zhang, X.; Zhang, G.; Qu, L. Two-Dimensional Nickel Porphyrinic Metal−Organic Framework-Modified Electrode for Electrochemical Sensing. *Langmuir* **2024**, *40* (5), 2708−2718.
(16) P, A. M.; R, A.; Haridas, S. Selective and Sensitive Non-Enzymatic Detection of Glucose by Cu(Ii)-Ni(Ii)/SBA-15. *New J. Chem.* **2024**, *48* (12), 5326−5333.
(17) Bano, M.; Naikoo, G. A.; BaOmar, F.; Rather, J. A.; Hassan, I. U.; Sheikh, R. A.; Kannan, P.; Tambuwala, M. M. Revolutionizing Glucose Monitoring: Enzyme-Free 2D-MoS2 Nanostructures for Ultra-Sensitive Glucose Sensors with Real-Time Health-Monitoring Capabilities. *ACS Omega* **2024**, *9* (18), 20021−20029.
(18) Gopal, T. S.; James, J. T.; Gunaseelan, B.; Ramesh, K.; Raghavan, V.; Malathi A, C. J.; Amarnath, K.; Kumar, V. G.; Rajasekaran, S. J.; Pandiaraj, S.; MR, M.; Pitchaimuthu, S.; Abeykoon, C.; Alodhayb, A. N.; Grace, A. N. MXene-Embedded Porous Carbon-Based Cu2O Nanocomposites for Non-Enzymatic Glucose Sensors. *ACS Omega* **2023**, *9* (7), 8448−8456.
(19) Guesmi, S.; Moulaee, K.; Bressi, V.; Kahri, H.; Khaskhoussi, A.; Espro, C.; Barhoumi, H.; Neri, G. Non-Enzymatic Amperometric Glucose Sensing by Novel Cu-MOF Synthesized at Room Temperature. *Mater. Adv.* **2024**, *5* (3), 1160−1170.
(20) Lima, R. N. S.; Del Colle, V.; Tremiliosi-Filho, G.; Angelucci, C. A. Unveiling the Effect of Pt Addition on Ag/C Catalyst for Enhanced Glycerol Electrooxidation. *Electrochim. Acta* **2024**, *489*, No. 144181.
(21) Medrano-Banda, A.; Ginoux, E.; Faverge, T.; Oshchepkov, A.; Bonnefont, A.; Chatenet, M.; Coutanceau, C.; Kéranguéven, G.; Cognet, P.; Savinova, E. Electrochemical Oxidation of Glucose in Alkaline Environment—A Comparative Study of Ni and Au Electrodes. *Electrochim. Acta* **2024**, *487*, No. 144159.
(22) Zhu, Z.; Qin, J.; Yang, Q.; He, H.; Yang, L.; Huang, H.; Ying, G. Interconnected Pd Nanowire Networks Stereoassembled on Biomass-Derived Porous Carbon Skeletons as Bifunctional Electrocatalysts for Efficient Methanol and Formic Acid Oxidation. *ACS Sustainable Chem. Eng.* **2024**, *12* (28), 10615−10623.
(23) Kang, K. N.; Kim, S. I.; Yoon, J. C.; Kim, J.; Cahoon, C.; Jang, J. H. Bi-Functional 3D-NiCu-Double Hydroxide@Partially Etched 3D-NiCu Catalysts for Non-Enzymatic Glucose Detection and the Hydrogen Evolution Reaction. *ACS Appl. Mater. Interfaces* **2022**, *14* (29), 33013−33023.
(24) Gu, Y.; Yang, H.; Li, B.; An, Y. A Ternary Nanocatalyst of Ni/Cr/Co Oxides with High Activity and Stability for Alkaline Glucose Electrooxidation. *Electrochim. Acta* **2016**, *192*, 296−302.
(25) Du, P.; Zhang, J.; Liu, Y.; Huang, M. Hydrogen Generation from Catalytic Glucose Oxidation by Fe-Based Electrocatalysts. *Electrochem. Commun.* **2017**, *83*, 11−15.
(26) Pavadai, R.; Amalraj, A.; Subramanian, S.; Perumal, P. High Catalytic Activity of Fluorophore-Labeled Y-Shaped DNAzyme/3D MOF-MoS2NBs as a Versatile Biosensing Platform for the Simultaneous Detection of Hg2+, Ni2+, and Ag+Ions. *ACS Appl. Mater. Interfaces* **2021**, *13* (27), 31710−31724.
(27) Pavadai, R.; Perumal, P. An Innovative Trimetallic-MOF Mediated Catalytic Cleavage Activity of FAM Tagged Ag10/T-Rich DNAzyme as an Ultra-Sensitive and Selective Fluorescent Biosensor for Subsequent Recognition of Ag+ and Hg2+ Ions. *J. Photochem. Photobiol., A* **2022**, *429* (December 2021), No. 113901.
(28) Amalraj, A.; Ayyanu, R.; Pavadai, R.; Govindaraj, T. S.; Aham, E. C.; Li, X.; Deng, Y.; Zhang, Z. Smartphone Assisted Paper Strip-Based Colorimetric Sensing of Phosphate and Copper Ions Utilizing Bi-Ligand Intercalated Cobalt-MOF as a Dual Functional Nanozyme. *J. Environ. Chem. Eng.* **2024**, *12* (5), No. 113522.
(29) Pavadai, R.; Perumal, P. Versatile Sensing Platform of an Innovative Copper Oxide-Assisted Cu-Phenolic Coordination Nanosheet-Mediated Fluorophore-Tagged GT-Rich SSA-Based Fluorescence ON-OFF Biosensor for the Subsequent Detection of Cd2+ and S2− Ions. *New J. Chem.* **2022**, *46* (7), 3431−3447.
(30) Jayaseelan, R.; Thennarasu, S.; Rajaji, P.; Nethaji, P.; Revathi, P.; Ramalingam, R. J.; Arokiyaraj, S. Long-Life Stability and High Energy Density Storage MnCoPB-PDA/NF Electrode Material in Hybrid Supercapacitors. *J. Energy Storage* **2023**, *72*, No. 108303.
(31) Zhao, H.; Tan, X.; Chai, H.; Hu, L.; Li, H.; Qu, L.; Zhang, X.; Zhang, G. Recent Advances in Conductive MOF-Based Electrochemical Sensors. *Chin. Chem. Lett.* **2024**, No. 110571.
(32) Baby, N.; Thangarasu, S.; Murugan, N.; Kim, Y. A.; Lee, J. M.; Oh, T. H. Versatile Bimetallic Metal-Organic Framework with Nanocutting Channels Tailored for Efficient Electrocatalytic Water Oxidation and Glucose Detection. *J. Alloys Compd.* **2024**, *970* (October 2023), No. 172601.
(33) Arivazhagan, M.; Pavadai, R.; Murugan, N.; Jakmunee, J. Surface Engineered Metal-Organic Framework-Based Electrochemical Biosensors for Enzyme-Mimic Ultrasensitive Detection of Glucose: Recent Advancements and Future Perspectives. *Anal. Methods* **2024**, *16* (38), 6474−6486.
(34) Chai, H.; Li, Y.; Yu, K.; Yuan, Z.; Guan, J.; Tan, W.; Ma, J.; Zhang, X.; Zhang, G. Two-Site Enhanced Porphyrinic Metal−Organic Framework Nanozymes and Nano-/Bioenzyme Confined Catalysis for Colorimetric/Chemiluminescent Dual-Mode Visual Biosensing. *Anal. Chem.* **2023**, *95* (44), 16383−16391.
(35) Li, Y.; Chai, H.; Yuan, Z.; Huang, C.; Wang, S.; Sun, Y.; Zhang, X.; Zhang, G. Metal−Organic Framework-Engineered Enzyme/Nanozyme Composites: Preparation, Functionality, and Sensing Mechanisms. *Chem. Eng. J.* **2024**, *496* (June), No. 153884.
(36) Subramanian, B. T.; Thomas, S.; Biju, V. M. N. Trifunctional Cobalt−Molybdenum Metal−Organic Framework for Electrochemical Oxygen Evolution Reaction and Aromatic Nitrosensing Applications. *J. Appl. Electrochem.* **2024**, *54* (3), 559−572.

https://doi.org/10.1021/acsomega.4c09437
ACS Omega 2025, 10, 1610−1623

(37) Shreyanka, S. N.; Theerthagiri, J.; Lee, S. J.; Yu, Y.; Choi, M. Y. Multiscale Design of 3D Metal−Organic Frameworks (M−BTC, M: Cu, Co, Ni) via PLAL Enabling Bifunctional Electrocatalysts for Robust Overall Water Splitting. *Chem. Eng. J.* **2022**, *446* (P2), No. 137045.
(38) Medina-Velazquez, D. Y.; Alejandre-Zuniga, B. Y.; Loera-Serna, S.; Ortiz, E. M.; de J Morales-Ramirez, A.; Garfias-Garcia, E.; Garcia-Murillo, A.; Falcony, C. An Alkaline One-Pot Reaction to Synthesize Luminescent Eu-BTC MOF Nanorods, Highly Pure and Water-Insoluble, under Room Conditions. *J. Nanopart. Res.* **2016**, *18* (12), No. 352.
(39) Zhang, C.; Wang, Q.; Zhang, W.; Li, X.; Zhu, Z.; Zhang, C.; Xie, A.; Luo, S. Preparation and Application of Co3O4-Ni-MOF/MWCNTs Hybrid for Supercapacitor. *Ionics* **2021**, *27* (8), 3543−3551.
(40) Bera, K.; Roy, S. S.; Madhu, R.; De, A.; Gudlur, P.; Kundu, S. Strategically Incorporated V in Rod-like Ni-MOF as an Effective Catalyst for the Water Oxidation Reaction. *Catal. Sci. Technol.* **2024**, *14* (10), 2858−2867.
(41) Arivazhagan, M.; Maduraiveeran, G. Ultra-Fine Nickel Sulfide Nanoclusters @ Nickel Sulfide Microsphere as Enzyme-Free Electrode Materials for Sensitive Detection of Lactic Acid. *J. Electroanal. Chem.* **2020**, *874*, No. 114465.
(42) Sultan, M. A.; Hassan, S. S.; Omran, K. A.; Hassan, H. B. A Novel Ni-Schiff Base Complex for Motivating Glucose Electro-oxidation in Alkaline Solutions. *Mater. Adv.* **2024**, *5* (3), 1264−1283.
(43) Pavadai, R.; Amalraj, A.; Perumal, P. A Cobalt-Based Bifunctional Metal Organic Framework-Mediated Fluorescent Bio-Sensing System for the Hypersensitive Detection of Ag+ Ions through Catalytic Hairpin Assembly. *New J. Chem.* **2022**, *46* (30), 14517−14531.
(44) Wang, Y.; Cao, W.; Wang, L.; Zhuang, Q.; Ni, Y. Electrochemical Determination of 2,4,6-Trinitrophenol Using a Hybrid Film Composed of a Copper-Based Metal Organic Framework and Electroreduced Graphene Oxide. *Microchim. Acta* **2018**, *185* (6), No. 315.
(45) Arivazhagan, M.; Maduraiveeran, G. Hierarchical Gold Dispersed Nickel Oxide Nanodendrites Microarrays as a Potential Platform for the Sensitive Electrochemical Detection of Glucose and Lactate in Human Serum and Urine. *Mater. Chem. Phys.* **2023**, *295* (August 2022), No. 127084.
(46) Arivazhagan, M.; Santhosh, Y. M.; Maduraiveeran, G. Non-enzymatic Glucose Detection Based on Nis Nanoclusters@nis Nanosphere in Human Serum and Urine. *Micromachines* **2021**, *12* (4), No. 403.
(47) Zhang, X.; Xu, Y.; Ye, B. An Efficient Electrochemical Glucose Sensor Based on Porous Nickel-Based Metal Organic Framework/Carbon Nanotubes Composite (Ni-MOF/CNTs). *J. Alloys Compd.* **2018**, *767*, 651−656.
(48) Hekmat, F.; Kachouei, M. A.; Taghadosi, S.; Shahrokhian, S.; Zhu, Z. Direct Decoration of Commercial Cotton Fabrics by Binary Nickel-Cobalt Metal-Organic Frameworks for Flexible Glucose Sensing in next-Generation Wearable Sensors. *Talanta* **2023**, *257* (February), No. 124375.
(49) Wang, X. Y.; Yan, X. X.; Wu, Y. P.; Wu, X. Q.; Yin, Y. M.; Li, S.; Zhang, Q.; Liu, B.; Li, D. S. Nonenzymatic Electrochemical Sensing Platform Based on 2D Isomorphic Co/Ni-Metal-Organic Frameworks for Glucose Detection. *Inorg. Chem.* **2023**, *62* (26), 10256−10262.
(50) Wei, X.; Guo, J.; Lian, H.; Sun, X.; Liu, B. Cobalt Metal-Organic Framework Modified Carbon Cloth/Paper Hybrid Electrochemical Button-Sensor for Nonenzymatic Glucose Diagnostics. *Sens. Actuators, B* **2021**, *329* (September2020), No. 129205.
(51) Ahmad, M. M.; Roushani, M.; Farokhi, S. Ni-P Nanosheets Derived from a Metal−Organic Framework Containing Triptycene Ligand: A High-Performance Electrochemical Sensor for Glucose Determination. *Microchem. J.* **2024**, *197* (November 2023), No. 109737.
(52) Zheng, W.; Liu, Y.; Yang, P.; Chen, Y.; Tao, J.; Hu, J.; Zhao, P. Carbon Nanohorns Enhanced Electrochemical Properties of Cu-Based Metal Organic Framework for Ultrasensitive Serum Glucose Sensing. *J. Electroanal. Chem.* **2020**, *862*, No. 114018.
(53) Xue, Y. T.; Chen, Z.; Chen, X.; Han, G. C.; Feng, X. Z.; Kraatz, H. B. Enzyme-Free Glucose Sensor Based on Electrodeposition of Multi-Walled Carbon Nanotubes and Zn-Based Metal Framework-Modified Gold Electrode at Low Potential. *Electrochim. Acta* **2024**, *483*, No. 144009.
(54) Sun, Y.; Li, Y.; Wang, N.; Xu, Q. Q.; Xu, L.; Lin, M. Copper-Based Metal-Organic Framework for Non-Enzymatic Electrochemical Detection of Glucose. *Electroanalysis* **2018**, *30* (3), 474−478.

https://doi.org/10.1021/acsomega.4c09437
ACS Omega 2025, 10, 1610−1623